Journal of Alloys and Compounds 509 (2011) L353–L358

Contents lists available at ScienceDirect

Journal of Alloys and Compounds

journal homepage: www.elsevier.com/locate/jallcom

Letter

Solution-phase chemical route to branched single-crystalline CdS nanoarchitectures and their field emission property

Ting Ge, Long Kuai, Baoyou Geng*

College of Chemistry and Materials Science, Anhui Key Laboratory of Functional Molecular Solids, Anhui Laboratory of Molecular-Based Materials, Anhui Normal University, Wuhu 241000, PR China

ARTICLE INFO

Article history:
Received 29 April 2011
Received in revised form 23 July 2011
Accepted 25 July 2011
Available online 3 August 2011

Keywords:
Single-crystalline CdS
Branched architectures
Solution-phase synthesis
Field emission

ABSTRACT

A facile solution chemical method is developed to prepare hierarchical branched single-crystalline CdS architectures. A mechanism of "nucleate-aggregate-grow-ripen-separate" process is proposed to illustrate the growth of the CdS architectures. The obtained branched CdS architectures exhibit superior FE properties with the lower turn-on field (Eto) of 7.1 V μm^{-1} at a current density of 10 $\mu A\,cm^{-2}$, and threshold field (Ethr) of 8.3 V μm^{-1} at a current density of 100 $\mu A\,cm^{-2}$, which shows that the obtained products have greatly potential application as FE devices.

1. Introduction

In recent years, extensive attention has been attracted to fabrication of semiconductors with controlled morphologies and sizes due to their greatly potential applications in many fields, such as photonics and electronics [1–5]. Notably, the nanostructured semiconductors based on the field-emission (FE) property are of great commercial interests in displays and other electronic devices, such as flat-panel displays, parallel-electron-beam microscopes, vacuum microwave amplifiers, and X-ray sources [6–10]. One-dimensional (1D) semiconductor nanostructures are pointed out to be ideal candidates as the optoelectronic devices and field emitters, for example, 1D ZnO, ZnS, CdS, and Si nanostructures, which have been achieved with a high FE-current density at low electric fields [11–16]. Especially, many researches suggested that branched nanostructures with a high packing density and highly crystalline nanotips could significantly enhance the FE properties and exhibit tremendous promise in single nanoscale transistors, electromechanical devices, and photovoltaics due to their excellent optical/electronic properties [17–37]. However, fabrication of hierarchical branched nanostructures with high packing density and highly crystalline nanotips has remained a challenge. The reported branched nanostructures often suffer from the small size (such as bipods, tripods, and tetrapods) and low packing density, which greatly limit their application as FE devices.

CdS, as an important semiconductor, has been proved to be one of the best promising FE candidates. The work function of CdS (4.2 eV) is lower than that of many other popular FE materials, such as carbon nanotubes (5.0 eV), ZnO (5.3 eV), and ZnS (7.0 eV). And the FE properties of 1D CdS nanostructures have been studied extensively, such as nanowire arrays [38], nanorod arrays [39] and nanobelts [40,41]. However, few reports are involved with the FE properties of hierarchical branched CdS nanostructures. Herein, well-defined hierarchical branched CdS nanostructures are fabricated by a solution chemical method. The products are typical branched structures with high yield, good uniformity and excellent crystallinity. In addition, the obtained branched CdS architectures exhibit superior FE properties with the lower turn-on field (Eto) of 7.1 V μm^{-1} at a current density of 10 $\mu A\,cm^{-2}$, and threshold field (Ethr) of 8.3 V μm^{-1} at a current density of 100 $\mu A\,cm^{-2}$, showing its greatly potential application as FE devices.

2. Experimental

2.1. Sample preparation

All chemicals are analytical grade and used without further purification. A hydrothermal method [42] is used to synthesize CdS nanostructures. Typically, 0.50 g $CdSO_4$ and 0.10 g $Na_2S_2O_4$ were dissolved into 20 mL distilled water to form a mixture. Then, 0.20 g cetyltrimethyl ammonium bromide (CTAB) was dissolved into 10 mL ethanol. Both solutions were continuously stirred for about 10 min respectively until clear solutions were obtained. Afterwards, they were mixed together slowly and kept vigorous stirring for 30 min. Finally, the obtained mixture was transferred into a 35 mL Teflon-lined stainless steel autoclave and maintained at 180 °C for 24 h. When the reaction finished, the autoclave was cooled to room temperature naturally. The yellow precipitate was collected, washed with distilled water and ethanol several times, and the final product was dried in a vacuum at 60 °C for 4 h.

* Corresponding author. Tel.: +86 553 3869303; fax: +86 553 3869303.
E-mail address: bygeng@mail.ahnu.edu.cn (B. Geng).

0925-8388/$ – see front matter © 2011 Elsevier B.V. All rights reserved.
doi:10.1016/j.jallcom.2011.07.094

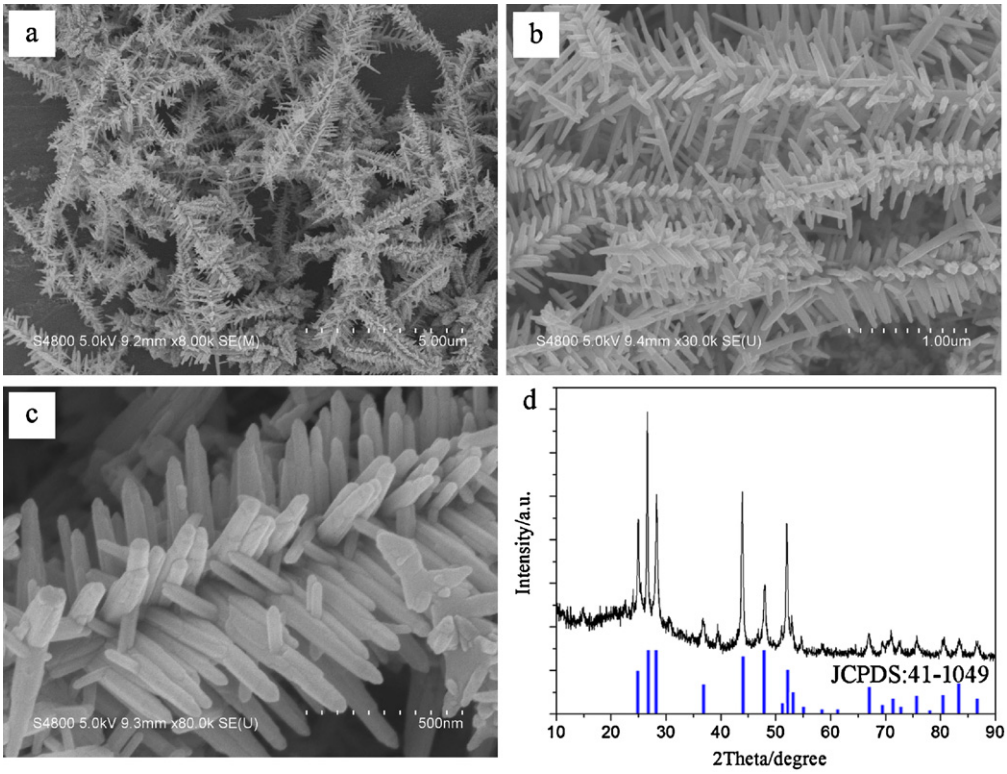

Fig. 1. Typical SEM images of the CdS nanoarchitectures obtained at 180 °C for 24 h. (a–c) SEM images of hierarchical CdS nanoarchitectures with different magnifications and (d) corresponding XRD pattern of the sample.

2.2. Characterizations

The samples were characterized by X-ray diffraction (XRD; Philips X'Pert with Cu Kα_1 radiation (λ = 0.154056 nm)), scanning electron microscopy (SEM; Hitachi S-4800, Japan), transmission electron microscopy (TEM; JEM 2010 F), high-resolution transmission electron microscopy (HRTEM; JEM 2010 F).

2.3. Field-emission measurements

Field-emission (FE) was measured in high vacuum chamber at a pressure of 2×10^{-6} Pa using a rod-like Cu probe with a cross-section of 1 mm^2 as anode, and the dendritic CdS microstructures were fixed onto a copper stage with conductive glue as the cathode. A direct current (dc) voltage sweeping from 100 to 1100 V was applied to the probe to collect emitted electrons from the ground cathode samples, and a corresponding electrical current was recorded automatically. The emission current density versus the applied field (J–E) curve was obtained at a working sample-anode distance of 100 μm from the dendritic-like CdS microstructures.

3. Results and discussion

Previously, thiosemicarbazide and thiourea are mainly used as sulfide resources to fabricate branched CdS nanostructures. It was thought that hydrogen-bond was necessary for the formation of the novel branched patterns. In those procedures, although many surfactants were used to control the morphology, such as poly(ethylene glycol) (PEG) and cetylpyridinium chloride (CPC) [43–45], the morphologies of those samples were often irregular and the crystallinity was also imperfect. The above deficiencies may limit their properties as the field-emission devices. Herein, we use $Na_2S_2O_4$ as sulfide resource to fabricate hierarchical branched CdS nanostructures, and the reactions are displayed as follow:

$$CdSO_4 + 3Na_2S_2O_4 \rightarrow CdSO_4{\cdot}3Na_2S_2O_4 \quad (1)$$

$$CdSO_4{\cdot}3Na_2S_2O_4 \rightarrow CdS + Na_2SO_4 + 2Na_2SO_3 + 3SO_2 \quad (2)$$

During the process, $CdSO_4$ combines initially with $Na_2S_2O_4$ to form a type of double salt ($CdSO_4{\cdot}Na_2S_2O_4$). Under heating, the double salt $CdSO_4{\cdot}Na_2S_2O_4$ decompose to generate CdS nanoparticle. The nanoparticles gather together, and then begin to epitaxialy grow. The oriented growth makes the branched CdS with sharp tips, which play an important role in FE properties. In addition, $Na_2S_2O_4$ releases S^{2-} slowly as sulfide resources, which is beneficial to forming hierarchical branched CdS with good crystallinity.

Fig. 1a–c shows the typical SEM images of the sample synthesized by solution reaction of $CdSO_4$ and $Na_2S_2O_4$ at 180 °C for 24 h. As shown in Fig. 1a, the obtained products are uniform branched nanostructures with high yield. The length of the trunks in the branches reaches approximately 5 μm. The high-magnification SEM images in Fig. 1b and c clearly show that the secondary branches of the nanostructure have high packing density with the length in the range of 400–600 nm. Moreover, some thirdly branches with the length about 200–300 nm are also observed on the secondary branches.

The phase purity of the as-synthesized products is investigated by XRD. The XRD pattern in Fig. 1d shows that all diffraction peaks can be well indexed to the standard hexagonal wurtzite-structured CdS with lattice parameters of a = 4.14 Å and c = 6.72 Å (JCPDS card 41-1049). According to the peaks of XRD pattern, the peak intensity of (0 0 2) plan is comparatively strong, which is most probably related to the preferential crystal growth orientation along the c-axis.

Fig. 2 shows the corresponding TEM and HRTEM images of the as-prepared product. The low-magnification TEM image (Fig. 2a) of the typical hierarchical dendrite further exhibits the regularity of crystal morphology, suggesting high packing density nanorods with sharp nanotips growing on the trunk. In each dendrite, there are several secondary branches on the major trunk. These branches have uniform diameters about 50 nm and are evenly spaced on a stem with a regular periodicity. Besides, the HRTEM images (Fig. 2c and d) are taken out at the marked areas in Fig. 2b. The fringe spacing is 0.36 nm and 0.67 nm, which is indexed to (1 0 0) and (0 0 1) planet of CdS nanocrystals, respectively.

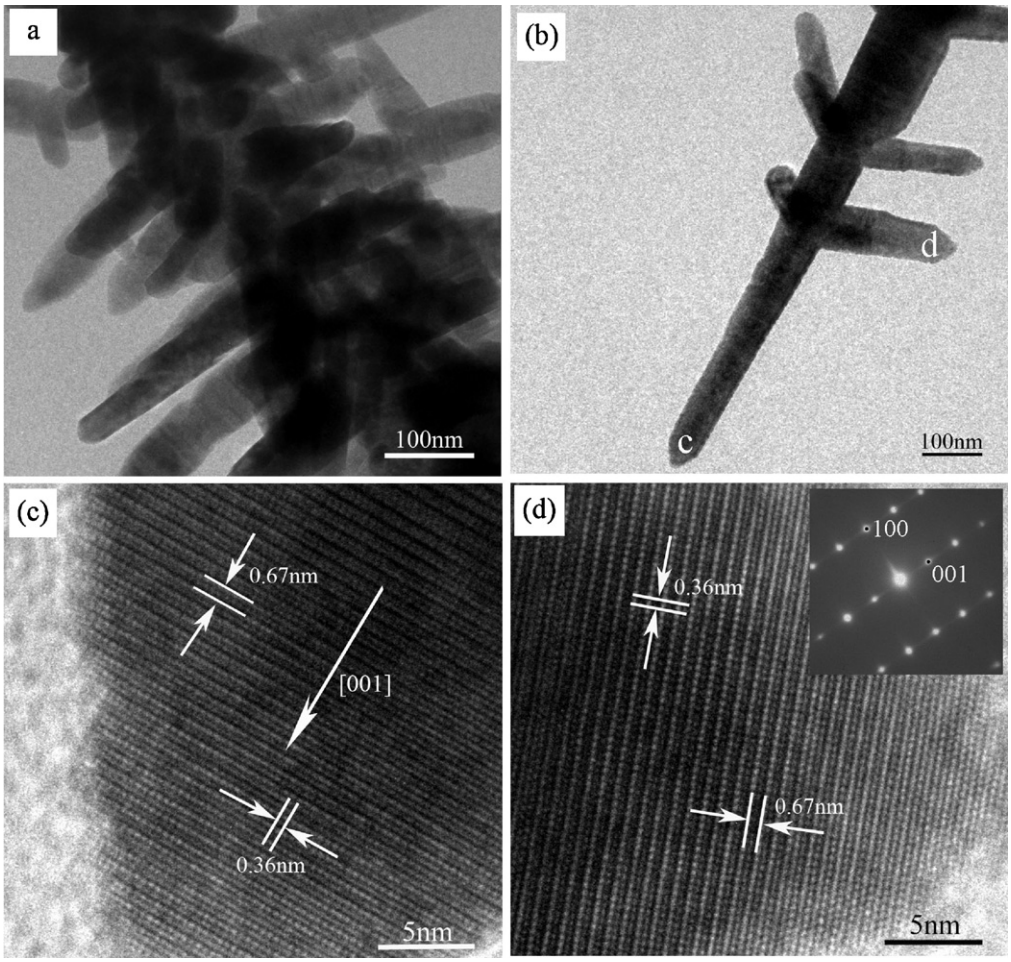

Fig. 2. Typical TEM images of the CdS nanoarchitectures. (a and b) TEM images of 3D dendritic CdS nanoarchitectures and (c and d) HRTEM image of each position of the individual dendritic CdS nanoarchitectures shown in (b), inset is the SAED pattern selected from (d).

Also, it can be easily found that the branch in an individual dendritic CdS nanoarchitecture is single crystalline and prefers to growth along the [0 0 1] direction, which coincides with the corresponding selected area diffraction (SAED) pattern (inset in Fig. 2d). The corresponding atomic schematic structural model of the branched CdS is displayed in Scheme 1. It shows that the single crystalline CdS prefers to grow along the [0 0 1] direction.

To investigate the formation process of the branched CdS, time-dependent experiments were carried out by keeping the other reaction conditions unchanged. The corresponding SEM images in Fig. 3 shows the morphologies of the products obtained at different reaction stages, which are corresponded to the reaction time of 0.5, 1, 10 and 24 h, respectively.

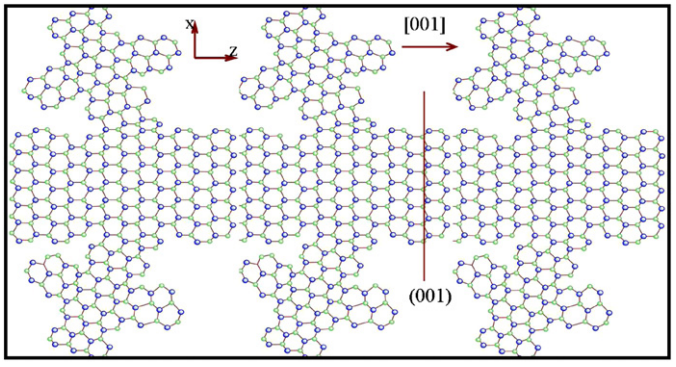

Scheme 1. The atomic schematic structural model of a dendritic CdS with the [0 0 1] growth direction (blue spheres represent Cd atoms and green ones are S atoms). (For interpretation of the references to color in this figure legend, the reader is referred to the web version of the article.)

At the early stage of the reaction (0.5 h), the obtained products are quasi-spheres with the diameter about 1 μm assembled by large numbers of small particles. When the reaction time is prolonged to 1 h, many branches with the length about 1–1.5 μm appear on the surface of the quasi-spheres. When the reaction time is further increased to 10 h, the length of the trunks and offshoots is both elongated obviously. The length of the trunks has reached to 2–4 μm and the secondary offshoots can be clearly observed. Several branches connect together and form shrubby morphology. Keeping on increasing reaction time to 24 h, it is found that the length of the branches reaches to 5 μm or longer and the branches separate from the roots of the shrubs. The corresponding XRD patterns of the time-dependent products suggest that the crystallinity of the products increases as the reaction time prolonged obviously, and the phase of the final products can be well indexed to the standard hexagonal wurtzite-structured CdS (JCPDS card 41-1049, see Fig. 4). The above results imply that the reaction time plays an important role in the growth of the branched achitechtures. In addition, the reaction temperature is one of the important factors in hydrothermal method. We found that the reaction temperature ranging from 160 °C to 200 °C is suitable to the formation of the branched CdS nanostructures, and the sample prepared at 180 °C is the most perfect one, so the reaction temperature at 180 °C was selected as the best condition.

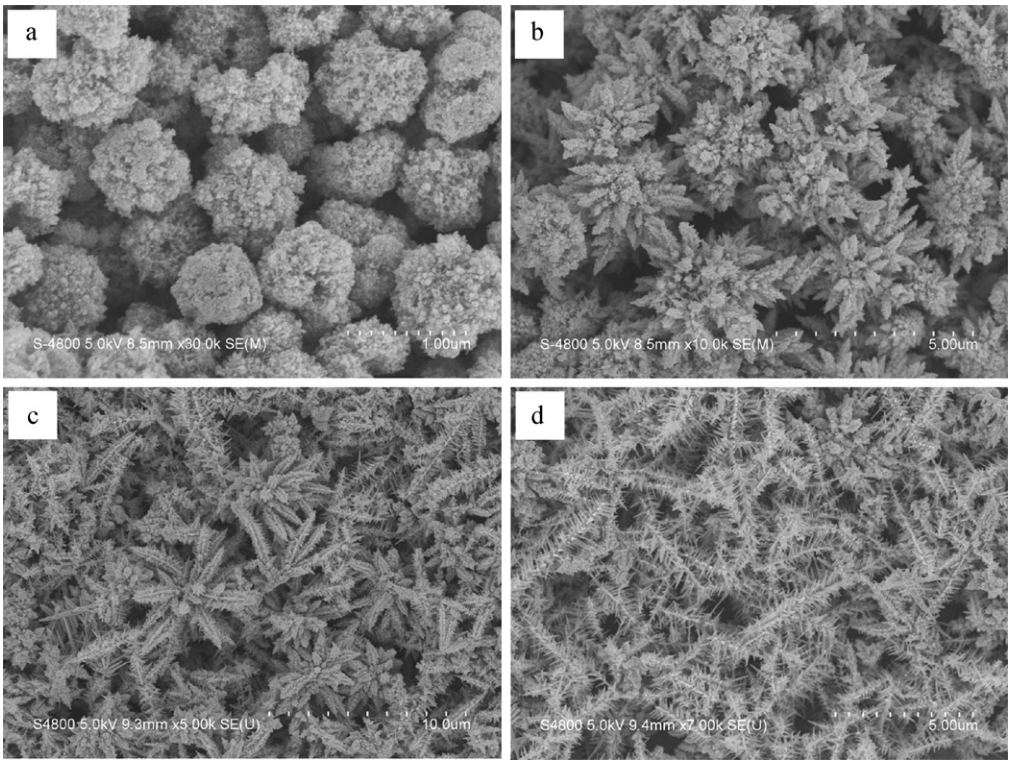

Fig. 3. FE-SEM images of 3D dendritic CdS nanoarchitectures obtained at different reaction times of (a) 0.5 h, (b) 1 h, (c) 10 h and (d) 24 h (all samples were prepared at 180 °C).

On the basis of above results, a type of "nucleate-aggregate-grow-ripen-separate" mechanism is proposed to explain the formation of branched CdS. Scheme 2 shows a growth schematic diagram of dendritic-like CdS nanoarchitectures.

(I) At the beginning of the reaction, $CdSO_4$ and $Na_2S_2O_4$ combine into a complex salt in reaction system. Under heating, the complex salt begins to decompose to generate CdS nanoparticles. The chemical reactions involved with this formation process have been illustrated previously (Eqs. (1) and (2)). (II) The cationic surfactant CTAB has played an important role in the growth of CdS nanocrystal. On the one hand, CTAB carries a positive charge in reaction solution, and it can effectively cap most surface of the newly formed CdS nanoparticles. On the other hand, the nitrogen atom in CTAB can form strong hydrogen-bond interaction among the CdS nanoparticles. As a result, the CdS nanoparticles assemble and form aggregates. (III) Diffusion-control growth thereafter occurs in the spherical aggregates as the nanoparticles are in close contact, and the surface area is reduced by nanoparticle fusion and structure rearrangement. At this stage, some spheres with a rough surface are obtained. (IV) Along with the reaction, the newly formed CdS grows out of the original spherical core, and extends toward favorable directions. The branched architectures are obtained after longer reaction time. (V) At the end of the reaction, the reactants have nearly been used up, central nucleus must be dissolved and the branches separate from each other. Therefore, a plenty of dispersive branched CdS nanostructures are generated.

The FE properties of the as-prepared branched CdS nanoarchitectures have been investigated, which are depicted in Fig. 5. Fig. 5a shows the emission current density versus the applied field (J–E) curve at a working sample-anode distance of 100 μm from the branched CdS nanostructures. With the increase of the applied field E, the emission current density J has exponentially increased. Based on Fig. 5a, the turn-on field (Eto), which is defined as an electric field

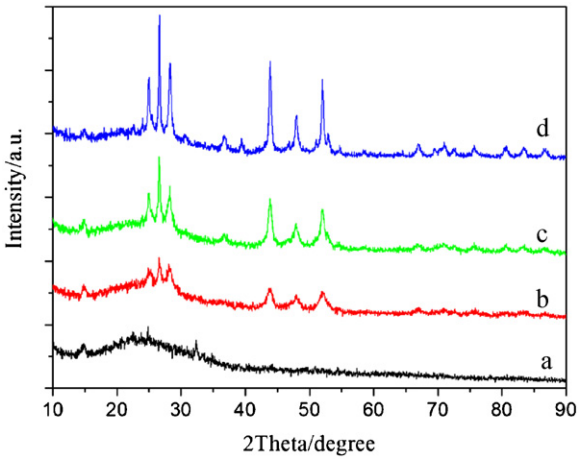

Fig. 4. XRD patterns of the products obtained with different reaction time. (a) 0.5 h, (b) 1 h, (c) 10 h and (d) 24 h.

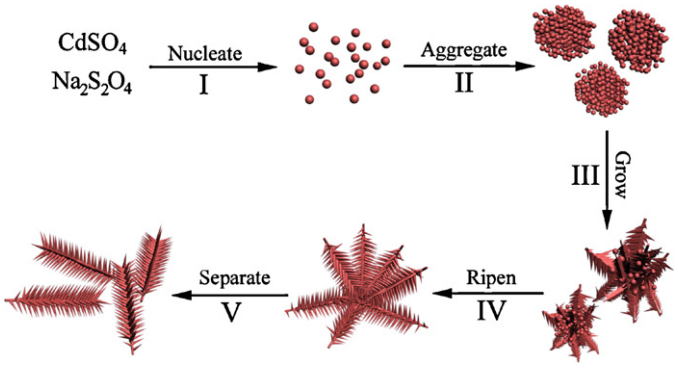

Scheme 2. Proposed growth process of the dendritic CdS nanoarchitectures.

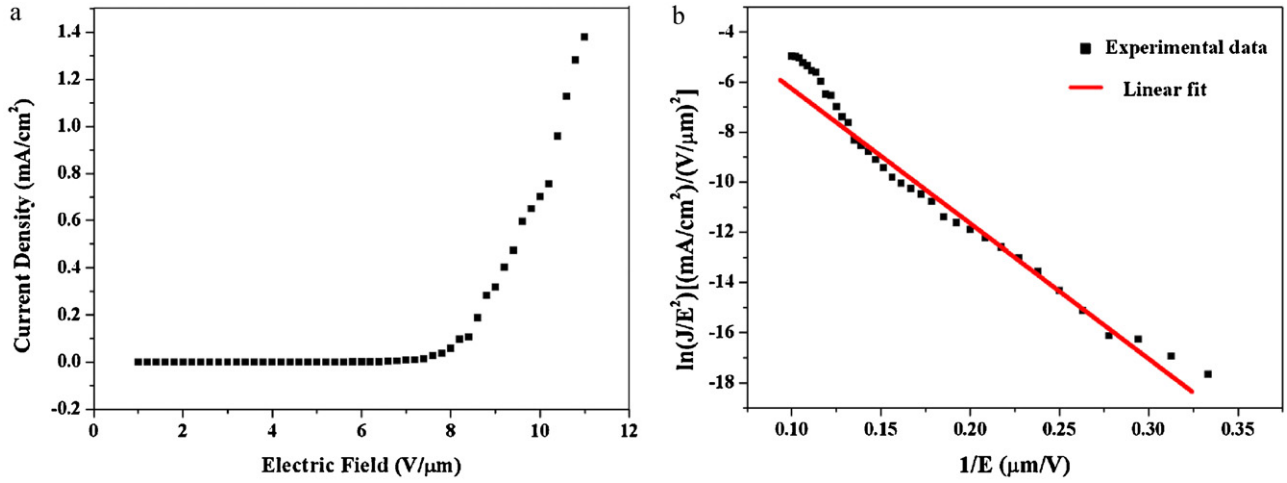

Fig. 5. Field-emission properties of dendritic-like CdS. (a) FE current density versus the applied field (*J*–*E*) curve at a working sample-anode distance of 100 μm. (b) The corresponding Fowler–Nordheim (F–N) plot of *J*–*E* curve showing a linear dependence.

to produce a current density of 10 μA cm^{-2}, is low at ~7.2 V μm^{-1}. The threshold field (Ethr) at a current density of 100 μA cm^{-2} is measured to be ~8.3 V μm^{-1}. The lower value of observed threshold field is attributed to the nanometric dimension and high aspect ratio of the compact CdS nanorods in branches. Similar to the previous reports of the CdS nanowires and nanorods, the as-prepared branched CdS nanoarchitectures with low turn-on field also can be used as practical field emitters.

The FE-current–voltage characteristics of the as-synthesized product are expressed based on the Fowler–Nordheim (FN) equation:

$$J = \left(\frac{A\beta^2E^2}{\varphi}\right)\exp\left(\frac{-B\varphi^{3/2}}{\beta E}\right) \quad (3)$$

$$\text{or} \quad \ln\left(\frac{J}{E^2}\right) = \ln\left(\frac{A\beta^2}{\varphi}\right) - \frac{B\varphi^{3/2}}{\beta E} \quad (4)$$

where J is the current density, E is the applied electric field, and φ is the work function of the emitting material, which is 4.2 eV for CdS. A and B are constants, in which $A = 1.54 \times 10^{-6}$ A eV V^{-2} and $B = 6.83 \times 10^3$ eV$^{-3/2}$ V μm^{-1}, respectively. The β is the field-enhancement factor, which have some connection with the emitter geometry (such as the aspect ratio), crystal structure, and spatial distribution of the emitting centers.

Fig. 5b illustrates the F–N plots for the branched CdS nanoarchitectures. The plots have an approximately linear relationship within the measurement range, demonstrating that the field-emission from CdS branched nanostructures behavior obeys the FN rule. Furthermore, the β value calculated from this equation is 1215, which is significantly larger than that of some other reported CdS nanostructures [31,32]. Herein, the superior field-emission property of the obtained nanostructures should be attributed to their original geometrical features.

4. Conclusions

In summary, we developed a facile and efficient solution-phase route to branched CdS nanoarchitectures. The obtained branched CdS structures possess large size, high packing density and highly crystalline nanotips, which are favorable to build FE emitters. The turn-on field (Eto) is low at 7.1 V μm^{-1} and the threshold field is 8.3 V μm^{-1} at a current density of 100 μA cm^{-2}, suggesting the greatly potential application as FE devices.

Acknowledgments

This work was supported by the National Natural Science Foundation of China (20671003, 20971003), the Key Project of Chinese Ministry of Education (209060), the Science and Technological Fund of Anhui Province for Outstanding Youth (10040606Y32) and the Program for Innovative Research Team at Anhui Normal University.

References

[1] J. Yang, C.H. Lin, Z.L. Wang, J. Lin, Inorg. Chem. 45 (2006) 8973.
[2] K.H. Park, K. Jang, S.U. Son, Angew. Chem. Int. Ed. 45 (2006) 4608.
[3] W.M. Qiu, M.S. Xu, X. Yang, F. Chen, Y.X. Nan, H.Z. Chen, J. Alloys Compd. 509 (2011) 8413.
[4] A.A. Yadav, E.U. Masumdar, J. Alloys Compd. 509 (2011) 5394.
[5] M. Cao, Y. Sun, J. Wu, X. Chen, N. Dai, J. Alloys Compd. 508 (2010) 297.
[6] H.B. Zeng, W.P. Cai, P.S. Liu, X.X. Xu, H.J. Zhou, C. Kingshirn, H. Kalt, ACS Nano 2 (2008) 1661.
[7] X.D. Bai, E.G. Wang, P.X. Gao, Z.L. Wang, Nano Lett. 3 (2003) 1147.
[8] Y. Jiang, W.J. Zhang, J.S. Jie, X.M. Meng, J.A. Zapien, S.T. Lee, Adv. Mater. 18 (2006) 1527.
[9] X.F. Duan, Y. Huang, R. Agarwal, C.M. Lieber, Nature 421 (2003) 241.
[10] L. Li, X.S. Fang, H.G. Chew, F. Zheng, T.H. Liew, X.J. Xu, Y.X. Zhang, S.S. Pan, G.H. Li, L.D. Zhang, Adv. Funct. Mater. 18 (2008) 1080.
[11] P. Ghosh, M.Z. Yusop, S. Satoh, M. Subramanian, A. Hayashi, Y. Hayashi, M. Tanemura, J. Am. Chem. Soc. 132 (2010) 4034.
[12] T.Y. Zhai, X.S. Fang, Y. Bando, B. Dierre, B.D. Liu, H.B. Zeng, X.J. Xu, Y. Huang, X.L. Yuan, T. Sekiguchi, D. Golberg, Adv. Funct. Mater. 19 (2009) 2423.
[13] T.Y. Zhai, M.F. Ye, L. Li, X.S. Fang, M.Y. Liao, Y.F. Li, Y. Koide, Y. Bando, D. Golberg, Adv. Mater. 22 (2010) 4530.
[14] M. Lei, P.G. Li, W.H. Tang, J. Alloys Compd. 509 (2011) 5020.
[15] J. Zhou, G.L. Zhao, J.J. Yang, G.R. Han, J. Alloys Compd. 509 (2011) 6731.
[16] J.F.A. Oliveira, T.M. Milão, V.D. Araújo, M.L. Moreira, E. Longo, M.I.B. Bernardi, J. Alloys Compd. 509 (2011) 6880.
[17] Z.G. Chen, L.N. Cheng, H.Y. Xu, J.Z. Liu, J. Zou, T. Sekiguchi, G.Q. Lu, H.M. Cheng, Adv. Mater. 22 (2010) 2376.
[18] L.W. Yin, Y. Bando, Y.C. Zhu, M.S. Li, Y.B. Li, D. Golberg, Adv. Mater. 17 (2005) 110.
[19] Y. Cui, U. Banin, M.T. Bjork, A.P. Alivisatos, Nano Lett. 5 (2005) 1519.
[20] L. Fang, J.Y. Park, Y. Cui, P. Alivisatos, J. Shcrier, B. Lee, L.W. Wang, M.J. Salmeron, J. Chem. Phys. 127 (2007) 184704.
[21] Y. Zhou, Y.C. Li, H.Z. Zhong, J.H. Hou, Y.Q. Ding, C.H. Yang, Y.F. Li, Nanotechnology 17 (2006) 4041.
[22] H.Z. Zhong, Y. Zhou, Y. Yang, C.H. Yang, Y.F. Li, J. Phys. Chem. C 111 (2007) 6538.
[23] S.H. Chen, Z.L. Wang, J. Ballato, S.H. Foulger, D.L. Carroll, J. Am. Chem. Soc. 125 (2003) 16186.
[24] S.D. Bunge, K.M. Krueger, T.J. Boyle, M.A. Rodriguez, T.J. Headley, V.L. Colvin, J. Mater. Chem. 13 (2003) 1705.
[25] L. Manna, D.J. Milliron, A. Meisel, E.C. Scher, A.P. Alivisatos, Nat. Mater. 2 (2003) 382.
[26] A. Fiore, R. Mastria, M.G. Lupo, G. Lanzani, C. Giannini, E. Carlino, G. Morello, M. De Giorgi, Y. Li, G. Cingolani, L. Manna, J. Am. Chem. Soc. 131 (2009) 2274.
[27] Y.C. Li, H.Z. Zhong, R. Li, Y. Zhou, C.H. Yang, Y.F. Li, Adv. Funct. Mater. 16 (2006) 1705.
[28] S. Kumar, T. Nann, Small 2 (2006) 316.

[29] Y.J. Na, H.S. Kim, J. Park, J. Phys. Chem. C 112 (2008) 11218.
[30] P. Peng, D.J. Milliron, S.M. Hughes, J.C. Johnson, A.P. Alivisatos, R.J. Saykally, Nano Lett. 5 (2005) 1809.
[31] L.W. Wang, J. Phys. Chem. B 109 (2005) 23330.
[32] M. Zhang, T.Y. Zhai, X. Wang, Y. Ma, J.N. Yao, Cryst. Growth Des. 10 (2010) 1201.
[33] Y.K. Tseng, C.J. Huang, H.M. Cheng, I.N. Lin, K.S. Liu, I.C. Chen, Adv. Funct. Mater. 13 (2003) 811.
[34] D. Banerjee, S.H. Jo, Z.F. Ren, Adv. Mater. 16 (2004) 2028.
[35] C.B. Cao, Z. Chen, X.Q. An, H.S. Zhu, J. Phys. Chem. C 112 (2008) 95.
[36] L. Carbone, S. Kudera, E. Carlino, W. Parak, J.C. Giannini, R. Cingolani, L. Manna, J. Am. Chem. Soc. 128 (2006) 748.
[37] U.K. Gautam, X.S. Fang, Y. Bando, J.H. Zhan, D. Golberg, ACS Nano 2 (2008) 1015.
[38] H.Y. Li, J.M. Green, J. Jiao, J. Phys. Chem. C 112 (2008) 15140.
[39] T.Y. Zhai, X.S. Fang, Y. Bando, Q. Liao, X.J. Xu, H.B. Zeng, Y. Ma, J.N. Yao, D. Golberg, ACS Nano 3 (2009) 949.
[40] T. Gao, Q.H. Li, T.H. Wang, Appl. Phys. Lett. 86 (2005) 173105.
[41] L. Li, P.C. Wu, X.S. Fang, T.Y. Zhai, L. Dai, M.Y. Liao, Y. Koide, H.Q. Wang, Y. Bando, D. Golberg, Adv. Mater. 22 (2010) 3161.
[42] M. Salavati-Niasari, F. Davar, M. Loghman-Estarki, J. Alloys Compd. 481 (2009) 776.
[43] D.J. Wang, D.S. Li, L. Guo, F. Fu, Z.P. Zhang, Q.T. Wei, J. Phys. Chem. C 113 (2009) 5984.
[44] X.J. Zhang, Q.R. Zhao, Y.P. Tian, Y. Xie, Cryst. Growth Des. 4 (2004) 355.
[45] Q.Q. Wang, G. Xu, G.R. Han, Cryst. Growth Des. 6 (2006) 1776.